Available online at www.sciencedirect.com
ScienceDirect
Journal of Molecular Catalysis A: Chemical 258 (2006) 221–230
JOURNAL OF MOLECULAR CATALYSIS A: CHEMICAL
www.elsevier.com/locate/molcata

Effect of the reduction–preparation method on the surface states and catalytic properties of supported-nickel particles

M. Cerro-Alarcón [a,b], B. Bachiller-Baeza [a,b], A. Guerrero-Ruiz [b,c], I. Rodríguez-Ramos [a,b,*]

[a] *Instituto de Catálisis y Petroleoquímica, CSIC, C/ Marie Curie no. 2, Campus de Cantoblanco, 28049 Madrid, Spain*
[b] *Grupo de Diseño y Aplicación de Catalizadores Heterogéneos, Unidad Asociada UNED-ICP (CSIC), Spain*
[c] *Departamento de Química Inorgánica y Química Técnica, Facultad de Ciencias, UNED, C/ Senda del Rey no. 9, 28040 Madrid, Spain*

Received 20 April 2006; received in revised form 18 May 2006; accepted 22 May 2006
Available online 3 July 2006

Abstract

Several high surface area graphite-supported Ni catalysts were prepared and reduced by different methods. Samples were prepared by impregnation of the support and then submitted to traditional H_2 flow reduction at high temperature or to reduction with aqueous hydrazine at low temperature, and compared with a sample prepared by the deposition–precipitation method by means of the reduction of the dissolved Ni precursor by hydrazine at low temperature. The surface of these catalysts was characterised by means of CO adsorption microcalorimetry and by X-ray photoelectron spectroscopy (XPS), and a correlation of the results obtained with those on the selective hydrogenation of citral can be done. In this sense, only Ni^0 sites were detected at the surface of the Ni catalysts prepared by reduction with hydrogen leading to high catalytic activities and selectivity towards citronellal formation, while Ni oxidised species are also present (and are major) for catalysts prepared by reduction with hydrazine, what leads to an enhanced selectivity towards the formation of the unsaturated alcohols, geraniol and nerol. The oxidation of these latter catalysts seems to be only superficial, as suggested by the absence of H_2 consumption peaks in the TPR experiments. The presence of Ni^0 sites over these latter catalysts was not detected by XPS, thus our study proves that CO adsorption microcalorimetry is a very powerful tool for surface characterisation of heterogeneous catalysts.

Keywords: Carbon-supported metal catalysts; High surface area-graphite; Nickel; Hydrazine; Surface characterisation; CO adsorption; Microcalorimetry; XPS; Citral hydrogenation

1. Introduction

It is noticeable how in the last years there has been an enhanced interest on the application of supported nickel catalysts. In this sense, heterogeneous Ni catalysts have been used in a variety of reactions such as reforming of methane [1,2], hydrogenolysis of hydrocarbons [3,4], and selective hydrogenations of aromatic rings and oxygenated compounds for the fine chemicals industry [5–7], among others. Most of these catalytic transformations have been seen to depend on the size, shape and structure of the metal particles, and thus on the electronic properties of the active sites. For such reasons, numerous studies have been devoted to the study of the parameters involved in the preparation of the catalysts. On supported metal catalysts one of these parameters, among others, is the reduction method, since it has an impact on the dispersion and final structure and electronic properties of the catalyst.

Conventional supported metal catalysts are usually prepared by *in situ* reduction at elevated temperatures of a metal salt. However, it is often difficult to control the size, structure and morphology of the final metal particles, particularly for impregnated catalysts [8], and rather heterogeneous distributions are achieved. In this way an alternative method for obtaining supported catalysts with well-defined metal particles is the preparation from metal colloids [9]. Besides, chemical methods have been developed to provide a better control of the structure at a microscopic level. In particular, reduction with hydrazine in aqueous or alcoholic media is receiving attention [9–12]. However, in spite of the numerous studies, a profound study concerning the surface active sites thus generated by this method is not available.

* Corresponding author. Tel.: +34 95854765; fax: +34 915854760.
E-mail address: irodriguez@icp.csic.es (I. Rodríguez-Ramos).

1381-1169/$ – see front matter © 2006 Elsevier B.V. All rights reserved.
doi:10.1016/j.molcata.2006.05.056

Among the many techniques available for surface characterisation of heterogeneous catalysts, adsorption microcalorimetry of probe molecules and X-ray photoelectron spectroscopy (XPS) are very powerful tools. The former can provide information on the energy of interaction of reactive molecules with the surface of the catalyst, which is a parameter related with its surface structure [13,14]. While the latter, can give useful information about the surface chemical state of the active sites of the catalysts. In this sense, the combination of both methods can provide quantitative information about the type and number of surface sites on the metal clusters. Moreover, the adsorption microcalorimetry technique provides more accurate adsorption heat values than those obtained from other techniques, and an energetic surface site distribution as a function of coverage may, thus, be obtained. However, adsorption microcalorimetry is scarcely applied to characterise metal supported catalysts [15].

In this work we have performed a surface analysis of high surface area graphite-supported Ni catalysts, prepared and activated (reduced) by several different methods, by CO adsorption microcalorimetry and X-ray photoelectron spectroscopy (XPS). Furthermore, the catalytic activity and selectivity of the samples were evaluated in the hydrogenation of the α,β-unsaturated aldehyde citral (3,7-dimethyl-2,6-octadienal). This compound can be used as a probe molecule in the liquid-phase hydrogenation, because it contains three unsaturated bonds including conjugated C=C and C=O bonds and an isolated C=C bond. Thus, the catalytic hydrogenation of these bonds results in different reaction selectivities depending on, for example, the reaction conditions [16], the metal precursor and support used in the preparation of the catalyst [17], the presence of promoters [18], etc. Hence, the catalytic properties are going to depend on the type and nature of surface sites of the catalyst. The final aim is to go deeply into the surface characterisation of the catalytic systems by determining the nature of the surface sites on Ni clusters supported on a high surface area graphite and generated from different preparation and reduction methods. In particular, our specific interest is to determine the type and nature of the surface sites generated by reduction with hydrazine alone, with no further reduction treatment, and to determine their catalytic properties. Comparison with a commercial Raney Ni catalyst and with catalytic samples activated by traditional hydrogen reduction will give us hints on the possible applications of such hydrazine reduced catalysts.

2. Experimental and methods

2.1. Catalyst preparation

A commercial high surface area graphite (HSAG-200, Lonza Ltd.), hereinafter named H, with specific surface area of 200 m^2/g and 3 wt.% oxygen content at surface, was used as support of Ni nanoparticles. Two different metal salts were selected as Ni precursors, $Ni(NO_3)_2{\cdot}6H_2O$ and $Ni(CH_3COO)_2{\cdot}4H_2O$. Nomenclature of the different graphite-supported Ni catalysts and a summary of the conditions used for their preparation (nickel precursor, preparation method, reducing agent, reduction temperature) are listed in Table 1. Two main methods were used for the preparation of the catalysts: the first one consisted on typical *impregnation* of the H support, in a rotator–evaporator, with an aqueous solution of the adequate quantity of the corresponding Ni precursor so as to obtain a 2 wt.% of Ni in the final catalysts. The samples so prepared were dried overnight in an oven at ca. 373 K and further submitted to *traditional reduction* (under flowing H_2 at 673 K for 2 h) or to *hydrazine reduction*, before characterisation or catalytic tests. Hydrazine reduction was performed in a five-necked glass reactor fitted with a stirred head, a thermometer, a reflux condenser, and a gas entry through a glass filter [19], and following a similar procedure as in [9,11,12]. Typically, about 3.0 g of the H-impregnated sample where suspended in 200 mL of doubly distilled water under flowing He atmosphere for 30 min, after which ca. 22 mL of hydrazine (85% aqueous solution $N_2H_4{\cdot}H_2O$; 55 wt.% N_2H_4; Sigma) where poured inside the reactor (pH of the final solution 10–11). Reduction was carried out at 353 K for ca. 3 h. The second preparation method consisted on the *in situ reduction* of the aqueous (dissolved) Ni precursor by aqueous hydrazine and *precipitation* of the so generated Ni nanoparticles over the H support (353 K, 3 h; flowing He atmosphere). This latter was also performed in the five-necked glass reactor using similar concentrations of reactants as described above and fitting both support and Ni precursor quantities to prepare a 2 wt.% loaded Ni catalyst. Catalysts prepared by the *impregnation-hydrazine reduction* method and by the *hydrazine reduction–precipitation method* (NiH–N–N_2H_4, NiH–A–N_2H_4 and NiH–A–N_2H_4P) were stored in the He-saturated aqueous media to prevent the oxidation of the Ni particles. The Raney Ni sample tested was a commercial one (>80 wt.% Ni, suspension in water; Fluka) and was used as will be specified later.

Table 1
Nomenclature and main preparation conditions of the high surface area graphite-supported nickel catalysts

Catalyst	Ni (wt.%)	Ni precursor	Reduction method
NiH–N-400	2	$Ni(NO_3)_2{\cdot}6H_2O$	H_2 flow at 673 K
NiH–N–N_2H_4	2	$Ni(NO_3)_2{\cdot}6H_2O$	N_2H_4 (ac) at 353 K
NiH–A-400	2	$Ni(CH_3COO)_2{\cdot}4H_2O$	H_2 flow at 673 K
NiH–A–N_2H_4	2	$Ni(CH_3COO)_2{\cdot}4H_2O$	N_2H_4 (ac) at 353 K
NiH–A–N_2H_4-200	2	$Ni(CH_3COO)_2{\cdot}4H_2O$	N_2H_4 (ac) at 353 K and H_2 flow at 473 K
NiH–A–N_2H_4P	2	$Ni(CH_3COO)_2{\cdot}4H_2O$	Reduction of salt (ac) by N_2H_4 (ac) at 353 K and DP[a] over H

[a] Deposition–precipitation.

2.2. Catalyst characterisation

2.2.1. Temperature-programmed reduction (TPR) experiments

Temperature-programmed reduction (TPR) measurements were carried out in a quartz micro-reactor over 200–300 mg of prepared impregnated sample and over catalysts prepared by the *impregnation-hydrazine reduction* and *hydrazine reduction–precipitation* methods, under a continuous flow of 20 cm^3/min of a H_2/Ar gas mixture (5% H_2). The temperature

was increased from room temperature up to 950 K at 2 K/min. H_2 consumption, as well as decomposition products (NO, CO, CO_2 and CH_4), were measured by on-line gas chromatography (Varian 3400) using a thermal conductivity detector (TCD).

2.2.2. CO adsorption microcalorimetry measurements

The CO chemisorption isotherms were determined volumetrically and the evolved heats in each pulse were measured simultaneously by means of a Tian Calvet heat-flow calorimeter (Setaram C-80 II) operated isothermally at 330 K and connected to a glass vacuum-dosing apparatus. Doses of approximately 2×10^{17} molecules of the probe gas were introduced into the system to titrate the surface of the metal catalysts. Both calorimetric and volumetric data were stored and analysed by microcomputer processing. The apparatus has been described in detail elsewhere [20]. The metal dispersions, D (%), were calculated from the total CO uptake at the monolayer (N_{ads}), considered to be attained when the evolved heat falls to the physisorption field (40 kJ/mol), and assuming a Ni:CO = 1:1 [21,22] stoichiometry. The mean crystallite sizes were calculated from dispersion values, assuming spherical metal particles, using the equation d (nm) = 1.01/D [23].

Manipulation of the samples, previous to these experiments, were different depending on the preparation and reduction method. Impregnated samples were *in situ* reduced under hydrogen flow at 673 K for 2 h, out-gassed (6.5×10^{-6} mbar) overnight at the same temperature, and cooled to 330 K. On the other hand, NiH–N–N_2H_4, NiH–A–N_2H_4 and NiH–A–N_2H_4P, as well as the Raney Ni sample, were dried and manipulated under inert (Ar) atmosphere in the calorimetric cell reactor previous to out-gassing overnight at 473 K. This temperature was chosen in order to avoid sintering of the metal particles. An experiment where sample NiH–A–N_2H_4 was reduced in flowing H_2 for 2 h previous to the out-gassing stage was also performed. The temperature for this reduction was the same as the one used for the vacuum treatment, 473 K.

2.2.3. X-ray photoelectron spectroscopy (XPS)

The surface chemical state of the catalysts was monitored by XPS with a VG-Microtech Multilab electron spectrometer using the Mg Kα radiation (1253.6 eV) from a twin anode in the constant energy analyser mode with a pass energy of 50 eV. The pressure in the analysis chamber was maintained at 5×10^{-10} mbar. The binding energy and Auger kinetic energy scale were set by assigning a value of 284.6 eV to the C 1s transition. The accuracy of the binding energy (BE) and Auger kinetic energy (KE) values were ±0.2 and ±0.3 eV, respectively. The BE and KE values were obtained by using the Peak-fit Program implemented in the control software of the spectrometer. Previous to these characterisation experiments, impregnated samples were reduced *in situ* (NiH–N-400 and NiH–A-400) in the pre-chamber of the apparatus, while NiH–N–N_2H_4, NiH–A–N_2H_4 and NiH–A–N_2H_4P were dried and pre-degassed in the pre-chamber of the apparatus (ca. 1×10^{-3} mbar) and further degassed in the transport chamber (ca. 1×10^{-8} mbar).

Determination of the surface composition of the catalysts was done by integration of the C 1s, Ni 2p, O 1s and N 1s regions, and using the corresponding sensitivity factors, after subtraction of the base line (non-linear Shirley type) and after a Gaussian–Lorentzian fitting of the peaks. For the analysis of the surface oxidation state, analysis of the Ni 2p level was done by fixing the distance between the Ni $2p_{3/2}$ and Ni $2p_{1/2}$ peaks at ca. 18.0 eV [24] and the satellites (when present) at ca. 6.0 eV from the corresponding photoelectron peaks [25].

2.3. Citral hydrogenation

The hydrogenation of citral was performed in a stainless steel batch reactor, operated at 5 MPa of H_2, at 323 K, using 0.4–0.5 g of reduced catalyst, 0.4–0.5 mL of citral, 100 mL of 2-propanol as the solvent, and keeping the system under continuous stirring of 500 rpm. Previous to the experiments, impregnated samples were treated at 673 K for 2 h under a continuous 20 cm^3/min H_2 flow (NiH-400 catalysts), while NiH–N–N_2H_4, NiH–A–N_2H_4, NiH–A–N_2H_4P, and the Raney Ni sample, were dried under inert atmosphere (Ar) followed by vacuum. All the catalysts were wetted with 2-propanol before transferring them to the batch reactor and then were kept within at 353 K under 5 MPa of H_2 overnight. Then, the reactor was cooled to the reaction temperature and citral was admitted into the reactor. Manual liquid samples were taken and analysed using a gas-chromatograph (Varian 3350) equipped with a flame ionisation detector (FID) and a capillary column. No mass transfer limitations occurred using the conditions described above. The initial intrinsic catalytic activity, A (μmol/g_{cat} s), was calculated from the slope of the linear region of conversion versus time plots.

3. Results and discussion

3.1. Temperature-programmed reduction (TPR)

Fig. 1 shows the TPR profiles of the H-supported Ni impregnated samples. The sample prepared from impregnation with $Ni(NO_3)_2 \cdot 6H_2O$ (NiH–N) shows two main reduction peaks at ca. 499 and 538 K, due to reduction of Ni^{2+} to Ni^0 species, as well as a broad band at ca. 623–841 K. The first H_2 consumption peak (ca. 499 K) appears along with a small quantity of CO_2, which can be assigned to the decomposition of the support's surface oxygen functional groups (carboxylic acid and lactone types), while peak at 538 K appears along with some CH_4 typical of the gasification of the support's surface carbon atoms. Higher amounts of CH_4 in addition to the hydrogen consumption band at 623–841 K are detected, in agreement with previous results obtained with a similar H-supported Ni catalyst [5]. Similar results are obtained for the sample prepared by impregnation with $Ni(CH_3COO)_2 \cdot 4H_2O$ (NiH–A). One main H_2 consumption peak at 582 K with a shoulder at ca. 565 K and a broad region at ca. 633–924 K are detected. In this case, very small amounts of CO_2 are detected (almost negligible), and CH_4 evolution together with H_2 consumption at 565 and 582 K may be ascribed to the decomposition and further reduction of the remaining acetate-type ligands of the precursor. Gasification of the support's surface carbon atoms would also take place at ca. 580 K but its extent would be larger for the 633–924 K region,

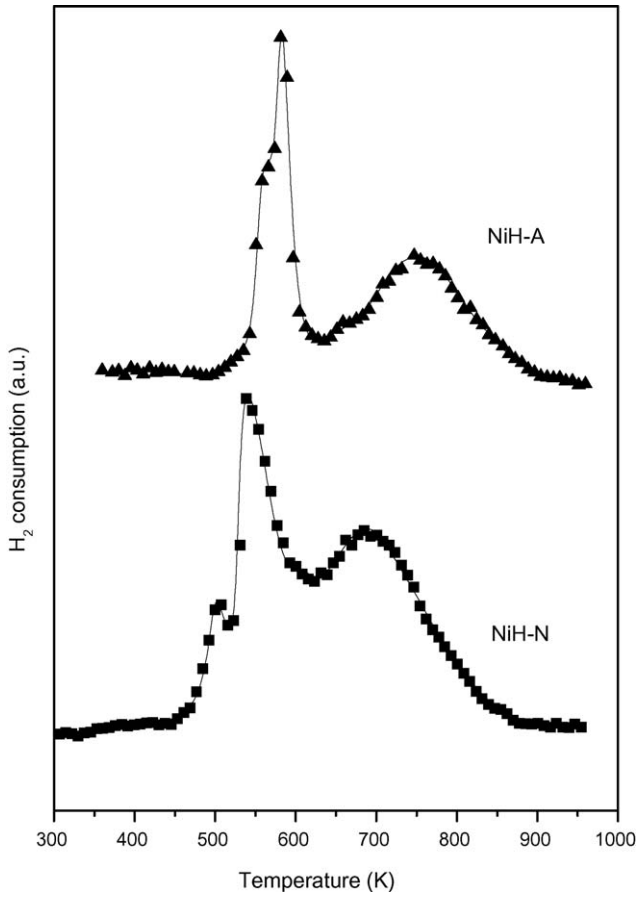

Fig. 1. Temperature-programmed reduction (TPR) profiles of H-impregnated Ni samples.

where a higher concentration of CH_4 is detected, in agreement with previous studies [5]. A precursor effect can be thus observed on the TPR profiles of these Ni samples. Reduction occurs at lower temperatures for NiH–N most probably due to the higher stability of $Ni(CH_3COO)_2$ type compounds respect to those of $Ni(NO_3)_2$. Also, crystallite size effects could account for this observation. When TPR experiments were performed over the NiH–N–N_2H_4, NiH–A–N_2H_4 and NiH–A–N_2H_4P samples no hydrogen consumption peaks were detected, indicating that Ni has been reduced by the hydrazine treatment as expected. In addition, no gases evolution from residual fragments of precursor (acetate or nitrate) on the hydrazine reduced catalysts was detected. This is different to that reported for silica supported nickel catalysts [11] where the supported nickel particles remained inserted in an organic matrix after reduction of the nickel precursor with hydrazine. Likely the nature of the support, a metal oxide in the latter case, plays a key role in the stabilization of the organic fragments.

3.2. X-ray photoelectron spectroscopy (XPS)

XPS was used to provide information about the oxidation state and chemical composition of the surface of the catalysts. Table 2 shows the binding energy of the Ni $2p_{3/2}$ photoelectron peak along with the Ni/C surface atomic ratios of the

Table 2
X-ray photoelectron spectroscopy results obtained for the high surface area graphite-supported Ni catalysts

Catalyst	$(Ni/C)_{XPS}$	Ni $2p_{3/2}$ BE (eV)
NiH–N-400	0.0054	852.8
NiH–N–N_2H_4	0.0210	855.9
NiH–A-400	0.0085	852.6
NiH–A–N_2H_4	0.0126	855.8
NiH–A–N_2H_4P	0.0069	856.0

H-supported Ni catalysts as determined by XPS. We can see that the Ni/C atomic surface ratios follow the trend NiH–N–N_2H_4 > NiH–A–N_2H_4 > NiH–A-400 ≥ NiH–A–N_2H_4P ≥ NiH–N-400. This Ni/C ratio is related with the size of the nickel particles formed on the graphite. Thus, as smaller metal particles are present at the surface of the catalysts, a higher concentration of nickel atoms would be exposed and thus detected by XPS. Therefore from these data it can be inferred that the reduction with hydrazine conduces to better metallic dispersion. Fig. 2 shows the background subtracted Ni $2p_{3/2}$ XPS spectra obtained for the graphite supported-Ni catalysts. NiH–N-400 and NiH–A-400 show the Ni $2p_{3/2}$ peak centred at 852.8 and 852.6 eV (Table 2), respectively, typical of the presence of Ni^0 species [26–28]. On the other hand, a very different surface state can be observed for samples prepared by reduction with hydrazine. In this sense, the Ni $2p_{3/2}$ XPS peaks of

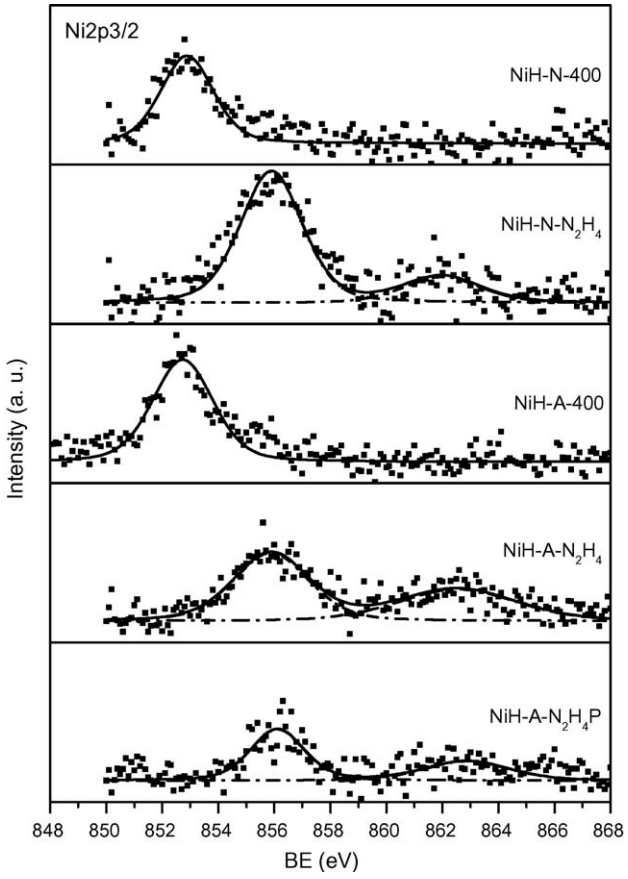

Fig. 2. XPS results: deconvolution of the Ni $2p_{3/2}$ level.

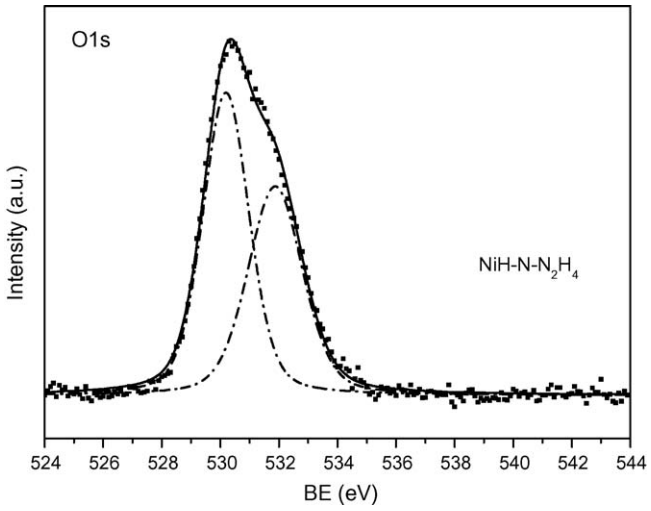

Fig. 3. XPS results for NiH–N–N_2H_4: deconvolution of the O 1s level.

NiH–N–N_2H_4, NiH–A–N_2H_4 and NiH–A–N_2H_4P are centred at ca. 855.9, 855.8 and 856.0 eV, respectively, that can be fitted with one contribution and assigned to Ni^{3+} species in Ni_2O_3 [26,29] and/or to Ni^{2+} as $Ni(OH)_2$ [29,30] or NiOOH [30]. Deconvolution of the O 1s XP peak (shown in Fig. 3 only for NiH–N–N_2H_4 for the sake of brevity), shows two contributions centred at ca. 530.2 and 531.9 eV. The 530.2 eV peak can be assigned to the presence of O^{2-} in NiO [26,27,30,31] and/or in Ni_2O_3 [26]. While peak at 531.9 eV could be due to Ni_2O_3 [24] and/or $Ni(OH)_2$ [24,26]. But, peaks between 529.9 and 532 eV have also been reported for oxygen species with single C–O and double C=O bonds present at the edge of the graphite layers on high-surface carbons [32]. Thus, as the oxygen content in the H support is around 3 wt.%, some contribution from the oxygen surface groups to the 531.9 eV peak is also expected. In any case, no Ni^0 species were detected for samples prepared-reduced with hydrazine, while Ni^{2+} and/or Ni^{3+} species seem to populate the surface of these catalysts. Even though the assignment of the specific oxidised Ni species is difficult due to the similarity in the binding energies (for both the Ni $2p_{3/2}$ and O 1s core levels), it can be inferred that surface oxidation is total in the case of NiH–N–N_2H_4, NiH–A–N_2H_4 and NiH–A–N_2H_4P as determined by XPS. Considering that no H_2 consumption peaks were detected by the TPR experiments we may say that oxidation is only superficial. No signals in the Ni $2p_{3/2}$ level can be assigned to residual acetate or nitrate (856.5 [33] and 856.8 eV [24], respectively) type compounds.

3.3. CO microcalorimetry measurements

Fig. 4A shows the CO differential adsorption heats versus coverage plots of the high surface area graphite-supported Ni samples after hydrogen reduction at 673 K, and of the Raney Ni bulk sample. We can see that the profiles are quite different, and typical of three heterogeneous surface site distributions. CO adsorption over Raney Ni results in an initial adsorption heat of ca. 124 kJ/mol that falls slowly to reach a value of ca. 105 kJ/mol at $\theta \sim 0.4$. Then, heats fall in a more sharp fashion until monolayer formation (ca. 40 kJ/mol). The initial adsorption heat of 124 kJ/mol would be in agreement with other studies carried out by other research groups for Ni powder (ca. 120 kJ/mol) [34]. In fact, it also fits well with those found in the literature for CO adsorption over the Ni (1 0 0) face arrangement: 125 kJ/mol [35], 120 kJ/mol [36] and 123 ± 2 kJ/mol [37]. Such heats may be ascribed to linearly adsorbed CO over metallic Ni sites (Ni^0–CO) as previously suggested for Ni powder [38]. The population of Ni sites strongly interacting with the CO molecule (ca. 125–105 kJ/mol) in the Raney Ni sample is high (ca. 40%), but since there is a strong fall of the adsorption heats for $\theta > 0.4$, a contribution of polycarbonylic species ($Ni^0(CO)_x$, $x = 2$ and/or 3) can also be considered. No bridged

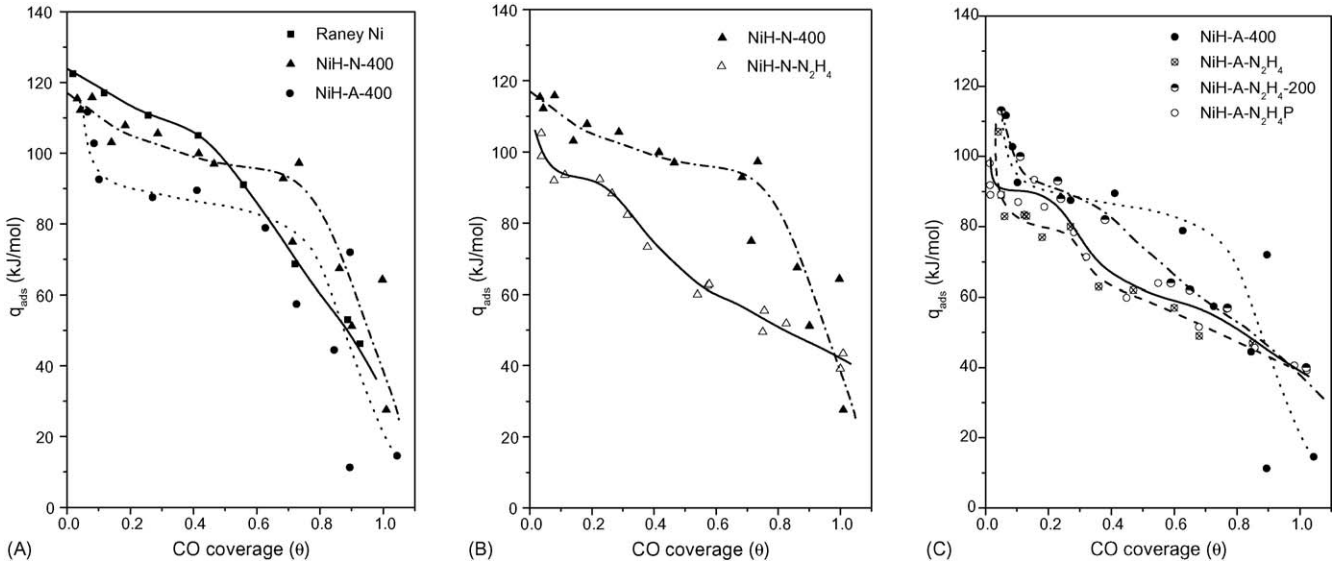

Fig. 4. Differential heats of CO adsorption at 330 K as a function of surface coverage: (A) Raney Ni and H-supported Ni catalysts reduced with hydrogen, (B) Ni catalysts prepared with $Ni(NO_3)_2{\cdot}6H_2O$, and (C) Ni catalysts prepared with $Ni(CH_3COO)_2{\cdot}4H_2O$.

CO species ($Ni_2(CO)$) seem to be formed since their formation over the Ni (1 0 0) face has been reported to give adsorption heats around 140–150 kJ/mol [39]. On the other hand, NiH–N-400 shows a CO adsorption microcalorimetric profile with an initial adsorption heat of ca. 117 kJ/mol that slowly falls to reach a value of ca. 97 kJ/mol at $\theta \sim 0.7$. Finally, heats sharply fall to the physisorption field (ca. 40 kJ/mol). The microcalorimetric profile obtained for this NiH–N-400 sample is comparable to those obtained with similar carbon-supported Ni catalysts [3,40]. Also, the initial CO adsorption heat of ca. 117 kJ/mol would fit with that reported for Ni powder (ca. 120 kJ/mol) [34] and with CO adsorption over the Ni (1 0 0) face [35–37]. Similarly as for the Raney Ni sample, such heats would be ascribed to linearly adsorbed CO over metallic Ni (Ni^0–CO) as suggested for Ni powder [38]. In the case of NiH–N-400, a contribution of polycarbonylic species ($Ni^0(CO)_x$; $x = 2$ and/or 3) can be considered too (taking into account that the heats of adsorption are slightly lower than those of Raney Ni). The formation of these polycarbonylic species have been previously suggested for alumina and silica-supported Ni catalysts [41]. NiH–A-400 shows a CO adsorption microcalorimetric profile with an initial adsorption heat of ca. 125–130 kJ/mol that sharply falls to ca. 90 kJ/mol at ca. $\theta = 0.18$. Then heats decrease again, but in a slower fashion, until ca. 80 kJ/mol at $\theta \sim 0.65$. Further increase in the surface coverage produces a sharp fall of the differential CO adsorption heats until monolayer formation. Formation of linear Ni^0–CO species seems possible, but it looks as though the surface of NiH–A-400 is covered mainly by $Ni^0(CO)_x$ ($x = 2$ and 3) polycarbonylic species.

XPS showed that both NiH–N-400 and NiH–A-400 exhibit Ni^0 sites, in agreement with CO adsorption microcalorimetry and with the literature. In addition, microcalorimetry shows different surface site distributions over the two NiH-400 samples, what is indicative of differences in the surface structure and/or morphology of the Ni^0 clusters, as previously suggested for carbon supported-Co catalysts [40], and that would be derived from the Ni precursor and its interaction with the support.

Fig. 4B and C show the CO differential adsorption heats versus coverage plots of the graphite-supported Ni catalysts prepared from the $Ni(NO_3)_2{\cdot}6H_2O$ (Fig. 4B) and $Ni(CH_3COO)_2{\cdot}4H_2O$ (Fig. 4C) precursors, comparatively for the different reduction/preparation methods (profiles of the hydrogen treated samples are again shown to enable comparison). Again, we can see profiles typical of heterogeneous surface site distributions, and that the microcalorimetric profiles are very different depending on both the preparation and the reduction method. NiH–N–N_2H_4 (Fig. 4B) shows a profile starting with a CO initial adsorption heat of ca. 108 kJ/mol that sharply falls until $\theta \sim 0.1$ at ca. 93 kJ/mol, where a very narrow plateau (coverage zone with a constant adsorption heat value) can be found ($\theta \sim 0.1$–0.22). Finally, heats fall again until the physisorption field is reached. Lower adsorption heats can be found for all the surface coverage range, compared to those of NiH–N-400, as expected considering the XPS results where no Ni^0 was detected for NiH–N–N_2H_4. However, the sample shows adsorption heats above 90 kJ/mol and a plateau at a q_{ads} value comparable to those obtained for NiH–N-400 and that were ascribed to linear and polycarbonylic species over Ni^0 sites. Thus, a small contribution of Ni^0 sites seems to be present at the surface of NiH–N–N_2H_4 despite the XPS results. This can be explained considering the measured signal for the whole XP spectra, which is very low and highly diffuse, and the low proportion of Ni^0 species, which is probably not enough to be detected. We can thus say that the surface of NiH–N–N_2H_4 is composed by a small contribution of Ni^0 sites that interact with the CO molecule by formation of linear (Ni^0–CO) and polycarbonylic species ($Ni^0(CO)_x$; $x = 2$ and/or 3), as previously ascribed for NiH–N-400. Adsorption heat values obtained for $\theta > 0.3$ would be due to the major formation of carbonylic species over oxidised Ni species (Ni^{2+} and Ni^{3+}), in agreement with XPS results and with the chemical nature of CO adsorption over transition metals (π-back donation to CO antibonding molecular orbitals is disfavoured from electron deficient metal sites). Heats of CO adsorption that can be found in the literature over NiO (1 0 0) are ca. 29–37 kJ/mol [42], determined by means of thermal desorption spectroscopy (TDS), and 43.7 kJ/mol by means of infrared reflection absorption spectroscopy (IRAS)–thermal programmed desorption (TPD) [43]. These data would be in general agreement with our results, considering the different characterisation techniques and the calculation errors of the TDS method. Besides, infrared–visible sum frequency generation (SFG) spectroscopy studies for adsorption of CO over NiO (1 1 1) reveal the formation of CO linear species over fully oxidised Ni^{2+} sites [44].

For NiH–A–N_2H_4 (Fig. 4C) something similar happens. This sample shows a profile with an initial adsorption heat of ca. 120 kJ/mol that sharply decays to reach a small plateau at ca. 80 kJ/mol comprising the $\theta \sim 0.1$–0.3 range. Finally, heats fall slowly to the weak-adsorption field. Again, a small proportion of Ni^0 seems to be present at the surface (linear Ni^0–CO and $Ni^0(CO)_x$), even though the major formation of carbonylic species over oxidised Ni species is apparent. Reduction of this sample under a H_2 flow at 473 K previous to the CO adsorption modifies the calorimetric profile. The initial heats of adsorption of 120–125 kJ/mol are similar to those obtained for the sample reduced directly at 673 K, NiH–A-400. As the coverage increased to 0.15, the heats of adsorption decreased sharply to 90 kJ/mol. After that, the heats decreased at a slower rate reaching the physisorption region. It is important to note that the heats of CO adsorption for this sample are higher than those obtained for the samples reduced only with hydrazine all over the range of coverage. Also, the general profile is very similar to that for NiH–A-400, although the progressive decay in the adsorption heats indicates that the sites are energetically more heterogeneous. Therefore, the two treatments at 473 K, vacuum or hydrogen flow, carried out over the hydrazine reduced samples generate different surface states. Although the reduction of the fresh sample starts at 550 K as we can see in the TPR (Fig. 1), the hydrogen treatment at 473 K seems to be enough to reduce the partially oxidised surface formed after the hydrazine reduction. The values for the heats of adsorption observed for this sample added to the higher amounts of adsorbed CO (Table 3) can corroborate that Ni is bulky reduced but partially oxidised on its surface in the samples treated with hydrazine.

Table 3
Catalytic properties in the hydrogenation of citral carried out at 323 K (conversion 40–45%)

Catalyst	N_{ads} (μmol/g)	A (μmol/g_{Ni} s)	Product distribution (selectivity, %)				
			S_{UOL}	S_{SAL}	S_{SOL}	$S_{3,7DMO}$	$S_{non\text{-}ident}$
NiH–N-400	12	187.0	0	93	2	2	3
NiH–N–N_2H_4	11	0.1	19	64	15	1	1
NiH–A-400	6	55.5	0	87	7	0	6
NiH–A–N_2H_4	9	0.2	21	49	23	6	1
NiH–A–N_2H_4-200	15	2.9	10	72	15	2	1
NiH–A–N_2H_4P	10	0.5	43	35	22	0	0
Raney Ni	360	33.1	1	74	17	8	0

For NiH–A–N_2H_4P, intermediate heats among those obtained for NiH–A-400 and NiH–A–N_2H_4 can be observed as well as a microcalorimetric profile typical of a more homogeneous surface site distribution. In this sense, two constant heat values (plateaux) are observed at ca. 90–92 and 60 kJ/mol for the 0.0–0.15 and 0.49–0.72 ranges, respectively. It can thus be inferred that two different types of Ni active sites for CO chemisorption are present at the surface of the NiH–A–N_2H_4P sample. The formation of polycarbonylic species over Ni^0 and carbonylic species over oxidised Ni sites seems most suitable. For this sample too, the apparition of a plateau at low q_{ads} indicates the interaction of the CO molecule with a specific oxidised Ni species.

The CO adsorption amounts (N_{ads}; μmol/g) values for the different nickel catalysts are shown in Table 3. Calculation of dispersion (D; %) and mean metal particle size (d; nm) was not performed considering that, as above described, several stoichiometries can occur during CO adsorption, such as M:CO = 1:1 (linear M–CO species), M:CO = 2:1 (bridged species M_2CO) or M:CO = 1:2 or 1:3 (polycarbonylic species $M(CO)_2$ or $M(CO)_3$), depending on both the Ni precursor used in the preparation of the samples and on the reduction method. Thus, in view of these factors calculation of accurate values for these catalysts is prone to error.

3.4. Citral hydrogenation

Data for intrinsic activity (A, μmol/g_{Ni} s) calculated as described in the experimental section, and selectivity towards the main hydrogenation products for a ca. 40–45% citral conversion: citronellal (SAL), nerol and geraniol (UOL), citronellol (SOL), 3,7-dimethyloctanol (3,7DMO), and other products (non-ident) such as isopulegol, acetal of citronellal, etc., are summarized in Table 3. It can be observed that the Raney Ni catalyst, along with the hydrogen reduced samples (NiH–N-400 and NiH–A-400), independently of the Ni precursor, show closer initial activity values. Furthermore, the activity of these three catalysts is several orders of magnitude higher than those observed for catalysts prepared by reduction with hydrazine (NiH–N–N_2H_4, NiH–A–N_2H_4 and NiH–A–N_2H_4P). For the latter catalysts the very low catalytic activity should be pointed out (the 40–45% citral conversion was achieved in several minutes, ca. 15–40 min, for the NiH-400 catalysts, while it took more than 3.5 days with the NiH–N_2H_4 catalysts). On the other hand, the activity for sample NiH–A–N_2H_4-200 is higher than that obtained for the sample reduced with hydrazine, but still lower than for NiH–A-400**.** These results indicate that the determining factor in the activity data is the reduction method employed and not the metal precursor. The metal precursor may have an impact on the surface structure and/or morphology of the metal particles as the microcalorimetry results may suggest, but activity depends on the quantity of completely reduced Ni^0 sites, in agreement with the characterisation of the catalysts, and as suggested elsewhere [45]. The microcalorimetry results have also indicated that samples reduced with hydrazine have a much lower contribution of Ni^0 species on the surface compared to catalysts reduced in hydrogen at 673 K. Also, it showed that the amount of these reduced species increases after the sample was subsequently reduced in H_2 at 473 K. Besides, it should be noted that no activation period for the NiH–N_2H_4 catalysts appeared. Thus, this would be in agreement with microcalorimetry where small concentrations of Ni^0 were detected, and discards the generation of new Ni^0 sites during the catalytic reaction.

On the other hand, in Table 3 it can also be observed that for Raney Ni and the hydrogen treated samples (independently of the Ni precursor), the main product generated in the hydrogenation of citral is citronellal (S_{SAL}). The formation and evolution of the reaction products with reaction time is consistent with the general scheme for the possible reactions for this hydrogenation process (Fig. 5). As can be seen in Fig. 6A for Raney Ni, formation of citronellal is maximum at total conversion of citral, and its concentration decreases as it is successively hydrogenated to citronellol. Moreover, citronellol and the total saturated alcohol, 3,7-dimethyloctanol are produced by the consecutive hydrogenation of citronellal and citronellol, respectively, even when citral has not been completely converted. In spite of the lower conversions obtained for the hydrazine reduced catalysts, a similar behaviour is observed for those catalysts as the profiles for NiH–N–N_2H_4 in Fig. 6B indicate.

On the other hand, NiH–N–N_2H_4, NiH–A–N_2H_4, and NiH–A–N_2H_4P generate an important amount of unsaturated alcohols geraniol and nerol (S_{UOL}), these amounts being very similar for the two former catalysts and lower than those obtained for the latter. For these three catalysts, the selectivity towards the different products is rather constant as conversion and time increase. The distribution of products observed for sample NiH–A–N_2H_4-200 clearly evidenced the influence of the reduction treatment, as occurred for the activity results. It can

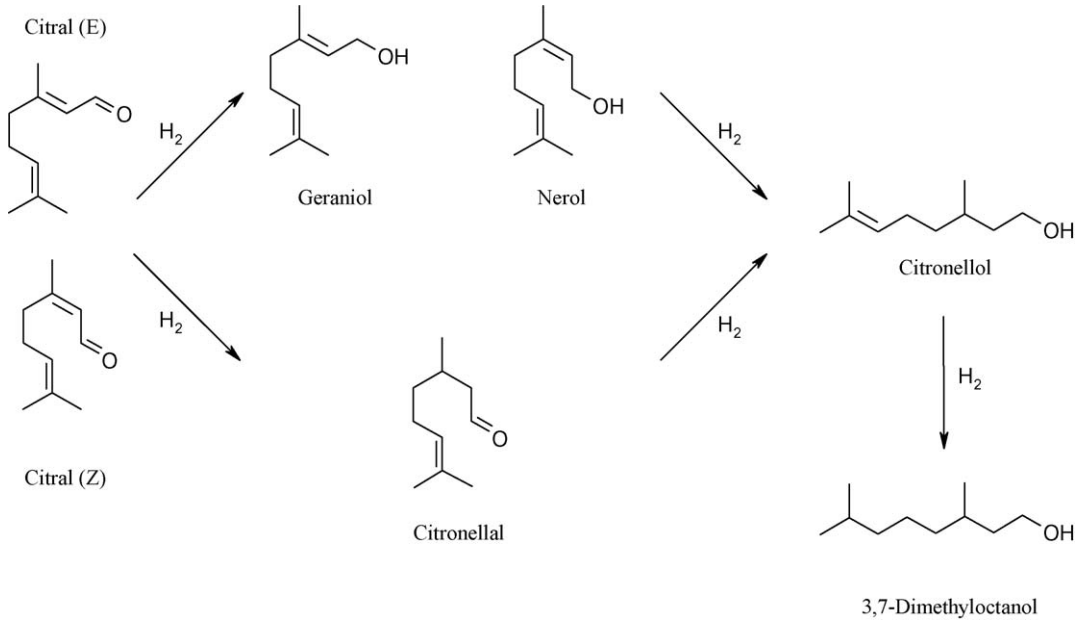

Fig. 5. Possible reactions in the hydrogenation of citral.

be seen in Table 3 that the selectivity to saturated aldehyde (S_{SAL}) has increased up to 72% at the expenses of the unsaturated alcohols, and approaching the values obtained with the sample reduced by the traditional method. Again, and similarly as for the activity data, selectivity towards the various products in the hydrogenation of citral seems to be related to the reduction method and to the Ni species present in the catalysts. As could be observed in the characterisation of the catalysts, the different reduction treatments generated different Ni species. This has been translated to different hydrogenation activities as a function of the surface Ni^0 species concentration (dissociation of the H_2 molecule proceeds over reduced metal sites), in agreement with CO adsorption microcalorimetry. However, the selectivity patterns observed for NiH–N–N_2H_4, NiH–A–N_2H_4 and NiH–A–N_2H_4P seem to be related to the oxidised Ni species. These species can activate the α,β-unsaturated aldehyde via the C=O bond, either acting as the electron-acceptor species and coordinating the oxygen atom of the substrate, or by polarization of the adsorbed substrate (through electronic interactions between oxidised Ni and Ni^0 species or by direct interactions between the oxidised Ni species and the adsorbate) [46, and references therein]. The higher selectivity to SAL for sample NiH–A–N_2H_4-200 agrees well with this assumption, since a lower proportion of oxidised Ni species exists on its surface compared to sample NiH–A–N_2H_4. In addition, we cannot rule out the fact that differences in the structure and/or morphology of the Ni particles induced by the different reduction and/or preparation methods, and evidenced by the microcalorimetry

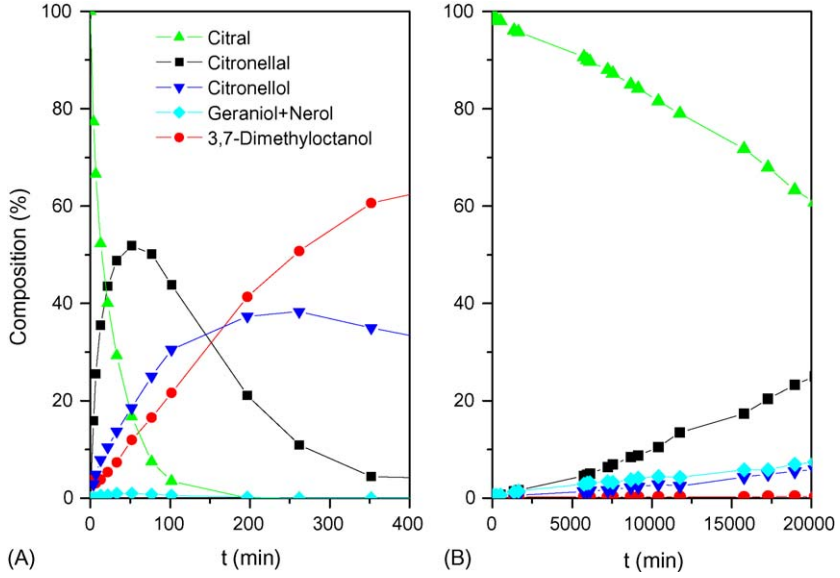

Fig. 6. Evolution of composition in the hydrogenation of citral for catalysts: (A) Raney Ni and (B) NiH–N–N_2H_4.

results, may have an influence on the selectivity results. The higher selectivity towards the unsaturated alcohols geraniol and nerol observed for NiH–A–N_2H_4P respect to those of the other NiH–N_2H_4 catalysts can be related to such differences.

4. Conclusions

The CO adsorption microcalorimetry technique provides, along with the identification of the Ni species by means of XPS, information that allows identification and quantification of the surface active sites. These data can be used to identify specific catalytic behaviours (activity and selectivity) in the hydrogenation of citral, and how such catalytic properties are modified when different surface sites are present at the surface of the catalysts.

The characteristics and properties of the high surface area graphite-supported Ni catalysts have been seen to depend (mainly) on the preparation-reduction method. Thus, reduction with hydrogen at high temperature (673 K) provides a surface constituted by Ni^0 sites only, while reduction with hydrazine at 353 K provides a surface constituted by low proportions of Ni^0 sites and mainly oxidised Ni^{2+} and/or Ni^{3+} species. The former implies high CO adsorption heats, due to formation of linear (Ni^0–CO) and polycarbonylic ($Ni^0(CO)_x$, $x=2$ and 3) species, and "high" activity in the hydrogenation of citral to yield citronellal and 3,7-dimethyloctanol. On the other hand, surface oxidation decreases the catalytic activity and favours the formation of the unsaturated alcohols (geraniol and nerol).

Besides, CO adsorption suggests that for NiH–A–N_2H_4 and NiH–A–N_2H_4P a specific oxidised Ni species (Ni^{2+} or Ni^{3+}) is prevalent at the surface. However, the higher concentrations of geraniol and nerol detected for NiH–A–N_2H_4P could be explained as a consequence of structural and/or morphological modifications on the Ni particles derived from the hydrazine reduction–precipitation method.

Acknowledgments

The financial support of the MC&T of Spain under projects MAT 2002-04189-C02-01 and MAT 2002-04189-C02-02. BBB would like to thank financial support from the Ministerio de Educación y Ciencia under the Ramón y Cajal Programme.

References

[1] P. Ferreira-Aparicio, A. Guerrero-Ruiz, I. Rodríguez-Ramos, Appl. Catal. A: Gen. 170 (1998) 177–187.
[2] O. Cherifi, M.M. Betahar, A. Auroux, Thermochim. Acta 306 (1997) 131–134.
[3] M. Cerro-Alarcón, A. Maroto-Valiente, I. Rodríguez-Ramos, A. Guerrero-Ruiz, Appl. Catal. A: Gen. 275 (2004) 257–269.
[4] M. Domingo-García, I. Fernández-Morales, F.J. López-Garzón, Appl. Catal. A: Gen. 112 (1994) 75–85.
[5] M. Cerro-Alarcón, A. Guerrero-Ruiz, I. Rodríguez-Ramos, Catal. Today 93–95 (2004) 395–403.
[6] A.F. Trasarti, A.J. Marchi, C.R. Apesteguía, J. Catal. 224 (2004) 484–488.
[7] P. Mäki-Arvela, L.-P. Tiainen, M. Lindblad, K. Demirkan, N. Kumar, R. Sjöholm, T. Ollonqvist, J. Väyrynen, T. Salmi, D.Y. Murzin, Appl. Catal. A: Gen. 241 (2003) 271–288.
[8] A. Miyazaki, I. Balin, K. Aika, Y. Nakano, J. Catal. 204 (2001) 364–371.
[9] A.G. Boudjahem, S. Monteverdi, M. Mercy, D. Ghanbaja, M.M. Bettahar, Catal. Lett. 84 (2002) 115–122.
[10] S.-H. Wu, D.-H. Chen, J. Coll. Interf. Sci. 259 (2003) 282–286.
[11] A.G. Boudjahem, S. Monteverdi, M. Mercy, M.M. Bettahar, J. Catal. 221 (2004) 325–334.
[12] A.G. Boudjahem, S. Monteverdi, M. Mercy, M.M. Bettahar, Catal. Lett. 97 (2004) 177–183.
[13] N. Cardona-Martinez, J.A. Dumesic, in: D.D. Eley, H. Pines, P.B. Weisz (Eds.), Advances in Catalysis, vol. 38, Academic Press, San Diego, 1992, pp. 149–224.
[14] P.J. Andersen, H.H. Kung, in: P.H. Emmett (Ed.), Catalysis, vol. 11, Athenaeum Press Ltd., The Royal Society of Chemistry, Newcastle, 1994, pp. 441–466.
[15] A. Guerrero-Ruiz, A. Maroto-Valiente, M. Cerro-Alarcón, B. Bachiller-Baeza, I. Rodríguez-Ramos, Top. Catal. 19 (2002) 303–311.
[16] L.-P. Tiainen, P.-M. Arvela, T. Salmi, Catal. Today 48 (1999) 57–63.
[17] G. Neri, L. Mercadante, A. Donato, A.M. Visco, S. Galvagno, Catal. Lett. 29 (1994) 379–386.
[18] B. Bachiller-Baeza, I. Rodríguez-Ramos, A. Guerrero-Ruiz, Appl. Catal. A: Gen. 205 (2001) 227–237.
[19] B. Bachiller-Baeza, A. Guerrero-Ruiz, P. Wang, I. Rodríguez-Ramos, J. Catal. 204 (2001) 450–459.
[20] B. Bachiller-Baeza, I. Rodríguez-Ramos, A. Guerrero-Ruiz, Langmuir 14 (1998) 3556–3564.
[21] E. Miyazaki, J. Catal. 65 (1980) 84–94.
[22] T. Narita, H. Miura, K. Sugiyama, T. Matsuda, R.D. Gonzalez, J. Catal. 103 (1987) 492–495.
[23] J.R. Anderson, Structure of Metallic Catalysts, Academic Press, New York, 1975, pp. 289–234.
[24] C.D. Wagner, W.M. Riggs, L.E. Davis, J.F. Moulder, in: G.E. Muilenberg (Ed.), Handbook of X-Ray Photoelectron Spectroscopy, Perkin-Elmer, Eden Prairie, Minnesota, 1979.
[25] P. Marcus, C. Hinnen, Surf. Sci. 392 (1997) 134–142.
[26] T.L. Barr, J. Phys. Chem. 82 (1978) 1801–1810.
[27] A.F. Carley, S.D. Jackson, J.N. O'Shea, M.W. Roberts, Surf. Sci. 440 (1999) L868–L874.
[28] E. Symianakis, S. Ladas, G.A. Evangelakis, Appl. Surf. Sci. 217 (2003) 239–249.
[29] D. Briggs, M.P. Seah, Practical Surface Analysis, vol. 1, 2nd ed., John Willey & Sons, 1993.
[30] J.-G. Kim, D.L. Pugmire, D. Battaglia, M.A. Langell, Appl. Surf. Sci. 165 (2000) 70–84.
[31] S.-J. Park, Y.-S. Jang, J. Coll. Interf. Sci. 263 (2003) 170–176.
[32] R.T.K. Baker, N. Rodriguez, A. Mastalir, U. Wild, R. Schlögl, A. Wootsch, Z. Paál, J. Phys. Chem. B 108 (2004) 14348–14355.
[33] L.J. Matienzo, L.I. Yin, S.O. Grim, W.E. Swartz, Inorg. Chem. 12 (1973) 2762–2769.
[34] B.E. Spiewak, J. Shen, J.A. Dumesic, J. Phys. Chem. 99 (1995) 17640–17644.
[35] J.C. Tracy, J. Chem. Phys. 56 (1972) 2736–2747.
[36] N. Al-Sarraf, J.T. Stuckless, C.E. Wartnaby, D.A. King, Surf. Sci. 283 (1993) 427–437.
[37] N. Al-Sarraf, D.A. King, Surf. Sci. 307–309 (1994) 1–7.
[38] J. Shen, B.E. Spiewak, J.A. Dumesic, Langmuir 13 (1997) 2735–2739.
[39] R.S. Bordoli, J.C. Vickerman, J. Wolstenholme, Surf. Sci. 85 (1979) 244–262.
[40] M. Cerro-Alarcón, A. Maroto-Valiente, I. Rodríguez-Ramos, A. Guerrero-Ruiz, Thermochim. Acta 434 (2005) 100–106.
[41] C.H. Bartholomew, R.B. Pannell, J. Catal. 65 (1980) 390–401.

[42] D. Capuz, J. Klinkmann, H. Kuhlenbeck, H.-J. Freund, Surf. Sci. 325 (1995) L421–L427.
[43] S.M. Vesecky, X. Xu, D.W. Goodman, J. Vac. Sci. Technol. A 12 (1994) 2114–2118.
[44] A. Bandara, S. Dobashi, J. Kubota, K. Onda, A. Wada, K. Domen, C. Hirose, S.S. Kano, Surf. Sci. 387 (1997) 312–319.
[45] J. Court, F. Janati-Idrissi, S. Vidal, in: M. Guisnet, et al. (Eds.), Heterogeneous Catalysis and Fine Chemicals II, Elsevier Science Publishers B.V., Amsterdam, 1991, pp. 193–200.
[46] P. Kluson, L. Cerveny, Appl. Catal. A: Gen. 128 (1995) 13–31.